Supplementary Information for

Thermodynamic and Achievable Efficiencies for Solar-Driven Electrochemical Reduction of Carbon Dioxide to Transportation Fuels

*Meenesh R. Singh, Ezra L. Clark, and Alexis T. Bell**

S-1 General Expression of Shockley-Queisser Limits of Multi-junction Light Absorbers

The Shockley-Queisser (SQ) limits of multi-junction light absorbers can be obtained as follows.(1, 2) Consider a stack of n light absorbers numbered from top to bottom in ascending order and decreasing band-gap energies. The JV characteristics of i^{th} light absorber at a fixed temperature can be obtained from the detailed balance, such that

$$J_i\left(E_{g,i},E_{g,i-1},V_i\right)=J_{\text{ph},i}\left(E_{g,i},E_{g,i-1}\right)+J_{\text{th},i}\left(E_{g,i},E_{g,i-1}\right)-J_{\text{rad},i}\left(E_{g,i},E_{g,i-1},V_i\right) \tag{1}$$

where J_i is the net current density, $J_{\text{ph},i}$ is the current density due to absorption of solar radiation, $J_{\text{th},i}$ is the current density due to absorption of thermal radiation, $J_{\text{rad},i}$ is the current density loss due to radiative emission, $E_{g,i}$ is the band-gap energy, and V_i is the bias developed across the i^{th} light absorber. The current density due to absorbed solar radiation is given as

$$J_{\text{ph},i}\left(E_{g,i},E_{g,i-1}\right)=\int_{E_{g,i}}^{E_{g,i-1}} I\left(E\right)dE \tag{2}$$

where $I\left(E\right)$ is a terrestrial air mass 1.5 spectrum of photon flux of energy E .(3) Note that the $E_{g,0}$ is infinity. The loss of current density due to radiation is given as

$$J_{\text{rad},i}\left(E_{g,i},E_{g,i-1},V_i\right)=\frac{e\left(\text{n}_{i+1}^2+\text{n}_{i-1}^2\right)}{4\pi^2c^2\hbar^3}\left[\begin{array}{l}\left(E_{g,i}^2kT+2E_{g,i}k^2T^2+2k^3T^3\right)\exp\left(\dfrac{eV_i-E_{g,i}}{kT}\right)-\\ \left(E_{g,i-1}^2kT+2E_{g,i-1}k^2T^2+2k^3T^3\right)\exp\left(\dfrac{eV_i-E_{g,i-1}}{kT}\right)\end{array}\right] \tag{3}$$

where e is the electronic charge, n_i is the refractive index of the i^{th} light absorber, c is the speed of light in vacuum, $\hbar$ is the reduced Planck constant, k is the Boltzmann constant, and T is the temperature. Consequently, the current density due to absorbed thermal radiation is given by J_{rad} with $V=0$:

$$J_{\text{th},i}\left(E_{g,i},E_{g,i-1}\right)=J_{\text{rad},i}\left(E_{g,i},E_{g,i-1},0\right) \tag{4}$$

Substituting equations (2)-(4) in equation (1) and rearranging the terms will give the diode equation (or the JV characteristics) of the i^{th} absorber.

$$J_i = J_{\text{sc},i} - J_{0,i}\left[\exp\left(\frac{eV_i}{kT}\right) - 1\right] \tag{5}$$

where $J_{\text{sc},i}$ is the short-circuit current density, and $J_{0,i}$ is the dark saturation current density of the i^{th} light absorber. It is clear that $J_{\text{sc},i} = J_{\text{ph},i}$ and $J_{0,i} = J_{\text{th},i}$. Since the current density through each light absorber in a stack should be same, their voltages can be added together to obtain the required expression for the JV characteristic of a multi-junction light absorber.

$$V(J) = \sum_{i=1}^{n} V_i = \frac{kT}{e}\sum_{i=1}^{n} \ln\left[\frac{J_{\text{sc},i} - J}{J_{0,i}} + 1\right] \tag{6}$$

The short-circuit current density and the open-circuit voltage of a multi-junction light absorber can be obtained as:

$$\begin{aligned} J_{\text{sc}} &= \min\left\{J_{\text{sc},1}, J_{\text{sc},2}, \cdots, J_{\text{sc},n}\right\} \\ V_{\text{oc}} &= \frac{kT}{e}\sum_{i=1}^{n} \ln\left[\frac{J_{\text{sc},i}}{J_{0,i}} + 1\right] \end{aligned} \tag{7}$$

S-2 Electrochemical Load Curve for IrO_2 Anode and Ag Cathode

The electrochemical loads (or current density versus voltage plot) are calculated for a cell containing IrO_2 anode and Ag cathode. The kinetics of CO2RR on Ag and the cell configuration was obtained from Hatsukade et al.(4) . Their electrochemical cell has 8 ml of 0.1 M $KHCO_3$ on each side of a Selemion AMV, continuously sparged with 20 cm^3 min^{-1} of CO_2, and an electrode area of 4.5 cm^2. The distance between the anode and cathode is ~3.56 cm. We use the Butler-Volmer expression to represent water oxidation kinetics for IrO_2 anode, where exchange current density is 1.4×10^{-4} mA cm^{-2}, anodic transfer coefficient is 1, and cathode transfer coefficient is 0.1. The electrochemical load curve is then calculated using the procedure described by Singh et al.(5)

Figure S1a shows the electrochemical load curve for CO and H_2 with the onset cell potential of 1.9 V. The current density of CO increases with the cell potential and reaches a plateau current density of 4.7 mA cm^{-2} at about 2.6 V. Thereafter, the current density of H_2 increases exponentially and that of CO decreases with the cell potential.

S-3 Electrochemical Load Curve for IrO_2 Anode and Cu Cathode

The electrochemical loads (or current density versus voltage plot) are calculated for a cell containing IrO_2 anode and Cu cathode. The kinetics of CO2RR on Cu and the cell configuration was obtained from Kuhl et al.(4) . Their electrochemical cell has 8 ml of 0.1 M $KHCO_3$ on each side of a Selemion AMV, continuously sparged with 20 cm^3 min^{-1} of CO_2, and an electrode area of 4.5 cm^2. The distance between the anode and cathode is ~3.56 cm. We use the Butler-Volmer expression to represent water oxidation kinetics for IrO_2 anode, where exchange current density is 1.4×10^{-4} mA cm^{-2}, anodic transfer coefficient is 1, and cathode transfer coefficient is 0.1. The electrochemical load curve is then calculated using the procedure described by Singh et al.(5)

Figure S1b shows the electrochemical load curve of various CO2RR products on Cu with the onset cell potential of 2.1 V. The current density of hydrogen and methane increases with the cell potential and reaches a maximum value of 9 mA cm^{-2} and 7 mA cm^{-2}, respectively. The current density of all other products shows maxima at intermediate cell potentials.

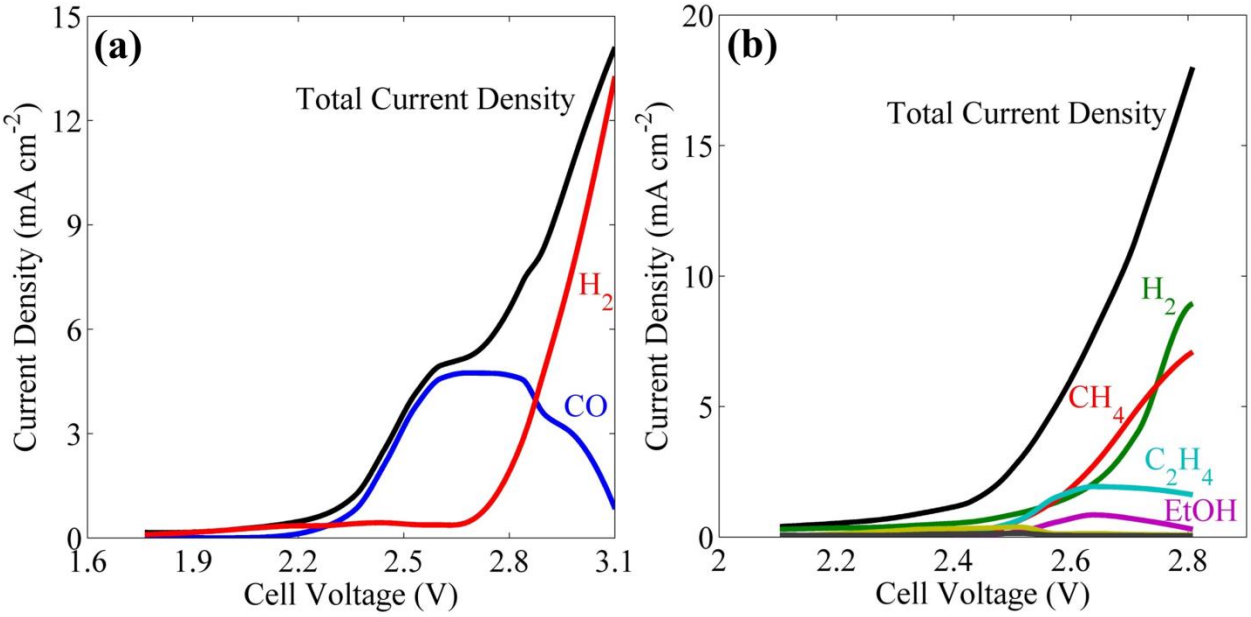

Figure S1: a) Electrochemical load curves of CO and hydrogen for IrO_2 anode and Ag cathode, (b) electrochemical load curves of hydrogen, methane, ethene, ethanol, formate (yellow, not labelled), CO (gray, not labelled) for IrO_2 anode and Cu cathode

S-4 Tandem Electrochemical Load Curves for IrO_2 Anode – Pt Cathode and Pt Anode – Ag Cathode

We consider two electrochemical cells in series – the first cell contains IrO_2 anode for OER and Pt cathode for HER, and the second cell contains Pt anode for HOR and Cu cathode for CO2RR. Hydrogen produced in the first cell is used in the second cell with CO_2 to produce

hydrocarbons. The kinetics of HER and HOR on platinum is represented by Butler-Volmer expression, where the exchange current density is 1 mA cm^{-2}, the anodic and cathodic transfer coefficients are 2.57. The electrochemical load curves for these cells are obtained for identical cell design and operating conditions as described in the sections S-2 and S-3. Figure S2a shows the typical electrochemical load curve for water-splitting (the first cell) and the Figure S2b shows electrochemical load curve for CO2RR (the second cell). The onset potential of the second cell is as low as 0.7V.

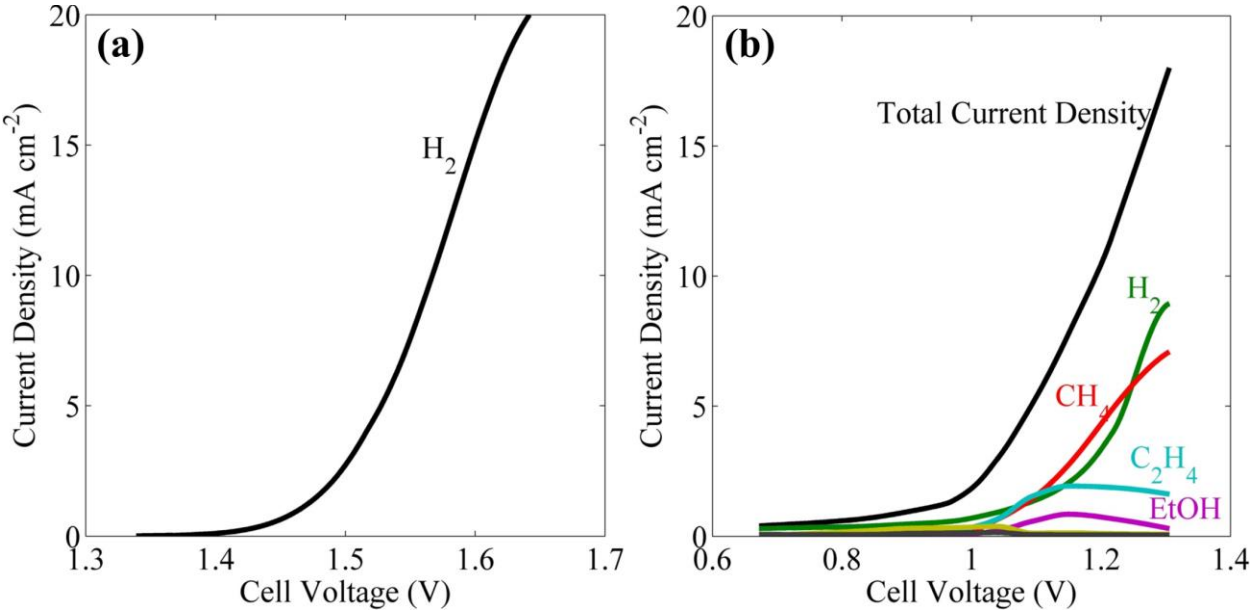

Figure S2: (a) Electrochemical load curve of a cell containing IrO_2 anode for OER and Pt cathode for HER, and (b) electrochemical load curve of a cell containing Pt anode for HOR and Cu cathode for CO2RR.

S-5 Optimal Band-Gaps for Multi-junction Light Absorber and their Panels

Figure S3a shows the optimal band-gap energies for single-, double-, and triple-junction light absorbers corresponding to the maximum current density given by solid-lines in Figure 2b. The optimal band-gap for a single-junction light absorber increases linearly at the rate of 0.13 eV V^{-1} with the electrochemical load causing a decrease in the fraction of the solar spectrum absorbed and, hence, in the current density. The optimal band-gaps for top and bottom junctions of double-junction light absorbers remain constant up to a load of 0.9 V and then increase steadily at the rates of 0.45 eV V^{-1} and 0.60 eV V^{-1}, respectively. The optimal band-gaps of top, middle, and bottom junctions of a triple-junction light absorber are constant up to a load of 1.95 V and thereafter increase at the rates of 0.246 eV V^{-1}, 0.337 eV V^{-1}, and 0.477 eV V^{-1}, respectively.

Figure S3b shows the optimal band-gaps and number of series connections for a panel of single- and double-junction light absorbers corresponding to the dotted-lines in Figure 2b. Figure S3b shows two, three, and four serially connected single-junction light absorbers can provide maximum current density in the load ranges 1.2 – 2.1 V, 2.1 – 3.05 V, and 3.05 – 3.5 V, respectively. In the case of double-junction light absorber, a single light absorber is efficient up to the load of 2.45 V and two serially connected light absorbers can be efficient in the load range of 2.45 – 3.5 V. Interestingly, the single light absorber with triple-junction does not require serial connections to boost its current density for the load range of 0.5 – 3.5 V.

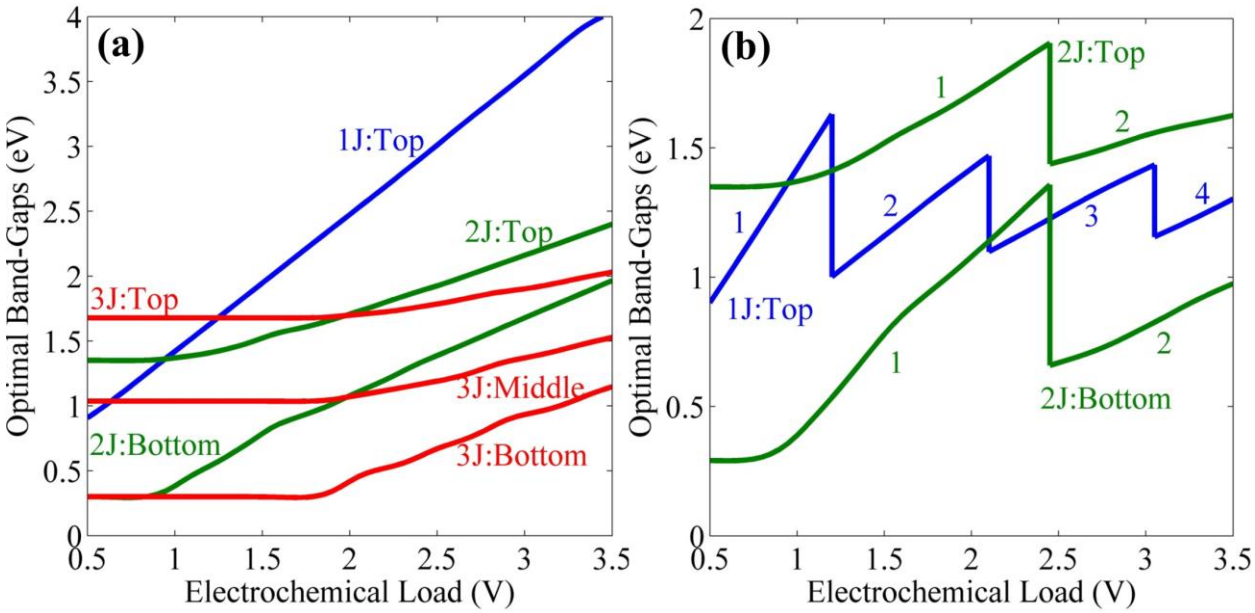

Figure S3: (a) Optimal band-gaps of a single-(blue), double-(green), and triple-(red) junction light absorber for various electrochemical loads, (b) optimal band-gaps of a panel of serially connected single-(blue) and double-(green) junction light absorbers, where numbers indicate serially connected light absorbers. 1J:Top denotes top band-gap of single-junction light absorber; 2J:Top and 2J:Bottom denote top and bottom band-gaps of double-junction light absorber, respectively; 3J:Top, 3J:Middle, and 3J:Bottom denote top, middle, and bottom band-gaps of triple-junction light absorber.

S-6 STF Efficiency of CO2R on Ag using Double-Junction Light Absorber

Figure S4 shows achievable STF efficiencies of H_2 and CO using silver cathode and ideal double-junction light absorber. The maximum total STF efficiency of 14%, which is a sum of 10% STF efficiency of H_2 and 4% STF efficiency of CO, is obtained for the top and bottom band-gaps of 2.15 eV and 1.65 eV, respectively. The maximum STF efficiency of CO of 6.95% can be obtained for several of combinations of band-gaps given by red contour in Figure S4b.

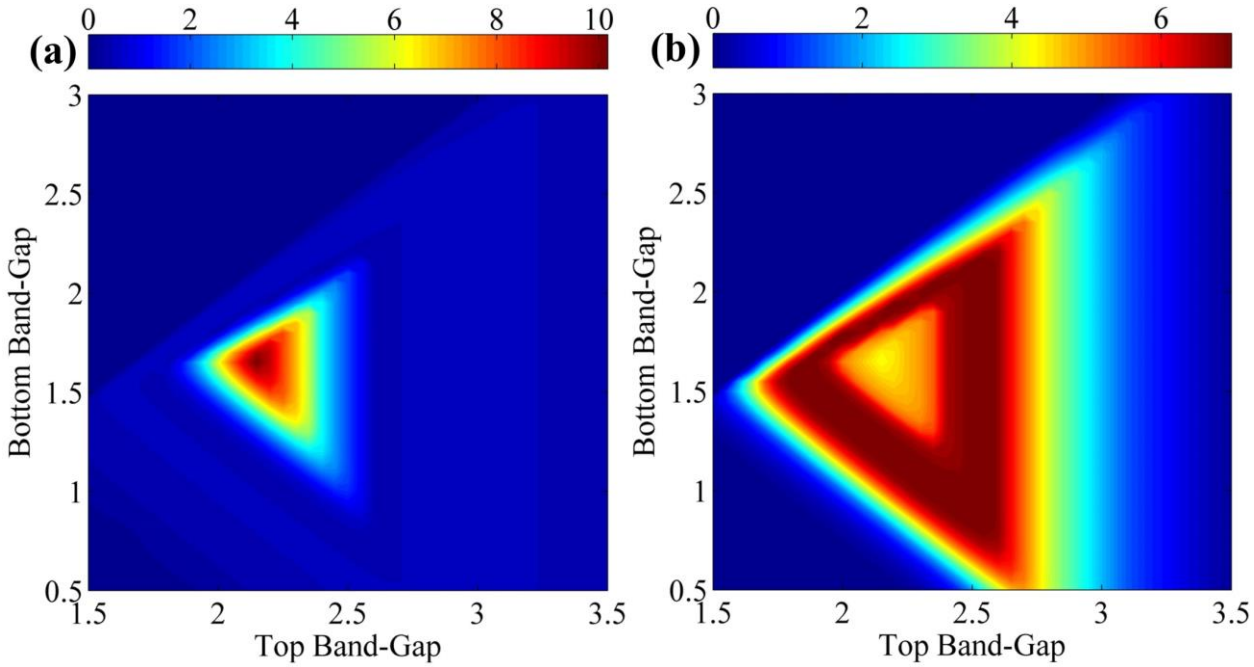

Figure S4: Achievable STF efficiencies of a) H_2 and b) CO formation on silver as a function of band-gaps of an ideal double-junction light absorber

S-7 STF Efficiency of CO2R on Cu using Double-Junction Light Absorber

Figure S5 shows achievable STF efficiencies of H_2, CH_4, C_2H_4, C_2H_5OH, $HCOO^-$ and CO using copper cathode and ideal double-junction light absorber. The maximum STF efficiency of Hythane® of 12.5% (out of a total STF efficiency of 15.4%) is obtained for top and bottom band-gaps of 2.05 eV and 1.55 eV, respectively. Their maximum STF efficiencies of other products such as 2.21% for C_2H_4, 0.91% for C_2H_5OH, 0.42% for $HCOO^-$, and 0.21% for CO can be obtained for several combinations of band-gaps of double-junction light absorber.

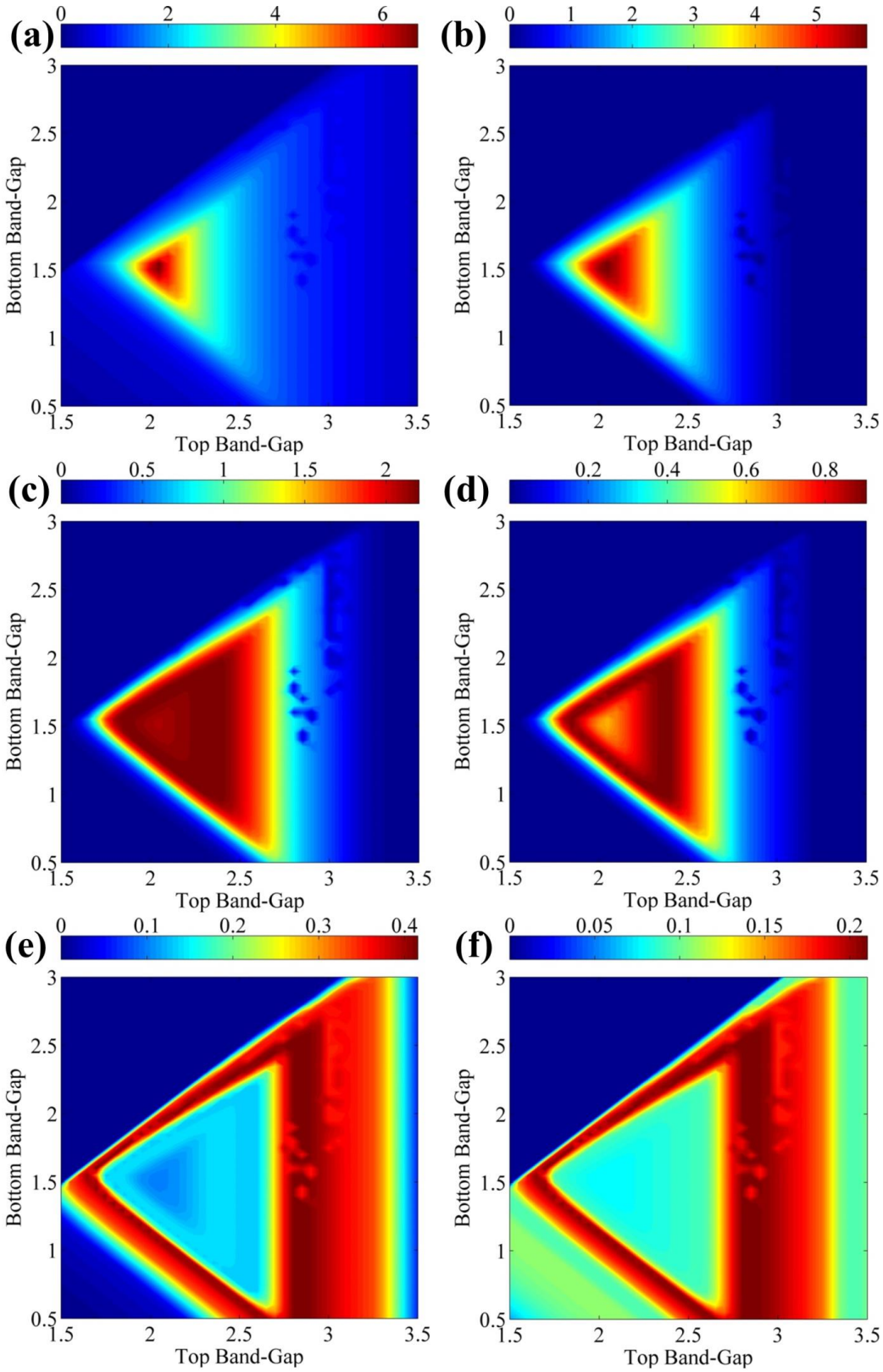

Figure S5: Achievable STF efficiencies of a) H_2, b) CH_4, c) C_2H_4, d) C_2H_5OH, e) $HCOO^-$, and f) CO formation on copper as a function of band-gaps of an ideal double-junction light absorber

S-8 STF Efficiency of CO2R on Cu using Triple-Junction Light Absorber

Figure S6 shows achievable STF efficiencies of minor products such as C_2H_4, C_2H_5OH, $HCOO^-$ and CO on copper cathode using an ideal triple-junction light absorber. Figure S6 shows contours of maximum STF efficiencies, as all the minor products show maxima in Figure S1b. Their maximum STF efficiencies are 2.21% for C_2H_4, 0.91% for C_2H_5OH, 0.42% for $HCOO^-$, and 0.21% for CO.

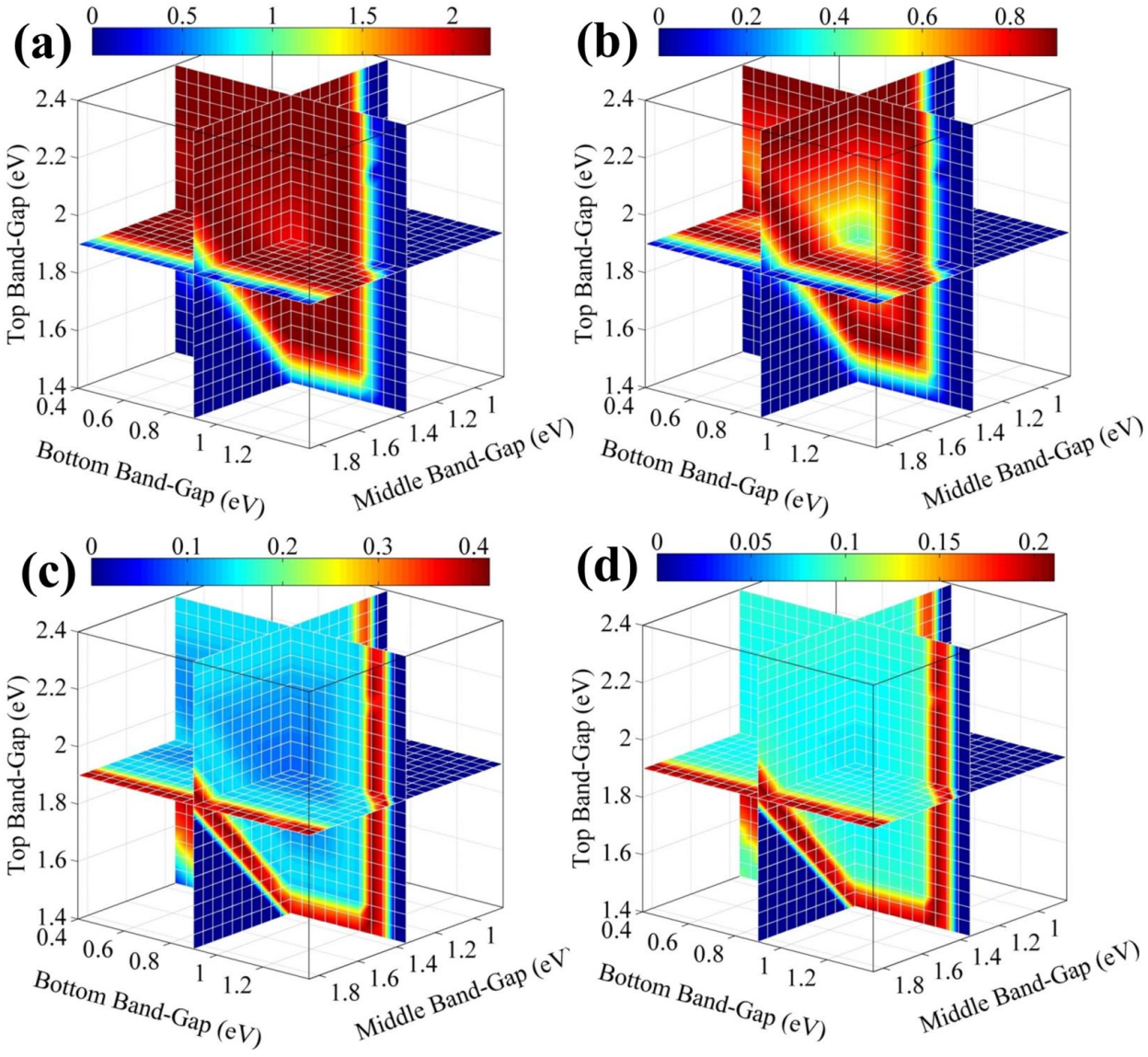

Figure S6: Achievable STF efficiencies of a) C_2H_4, b) C_2H_5OH, c) $HCOO^-$, and d) CO formation on copper as a function of band-gaps of an ideal triple-junction light absorber

S-9 JV Characteristics of Spectrolab's Triple-Junction Light Absorber

Figure S7a shows current density versus voltage (JV) characteristic of 28% efficiency InGaP/GaAs/Ge triple-junction light absorber measured at AM 1.5.(6) The triple-junction light absorber has short-circuit current density of 12.64 mA cm^{-2} and open-circuit voltage of 2.29 V. The fill factor of the measured JV curve is 0.756.

S-10 Effect of Ratio of Catalyst to PV Area on the Fuel Selectivity

Figure S7b shows the variation in the STF and faradaic efficiencies of CO formation with the ratio of catalyst to PV area of a PV-electrolyzer. The PV-electrolyzer has two InGaP/GaAs/Ge light absorbers (Figure S7a) connected in series with an electrochemical cell containing IrO_2 anode and Ag cathode. The PV-electrolyzer can operate at maximum STF efficiency of 8.6% and produce 92.6% pure CO, when the ratio of catalyst to PV area is 1.25.

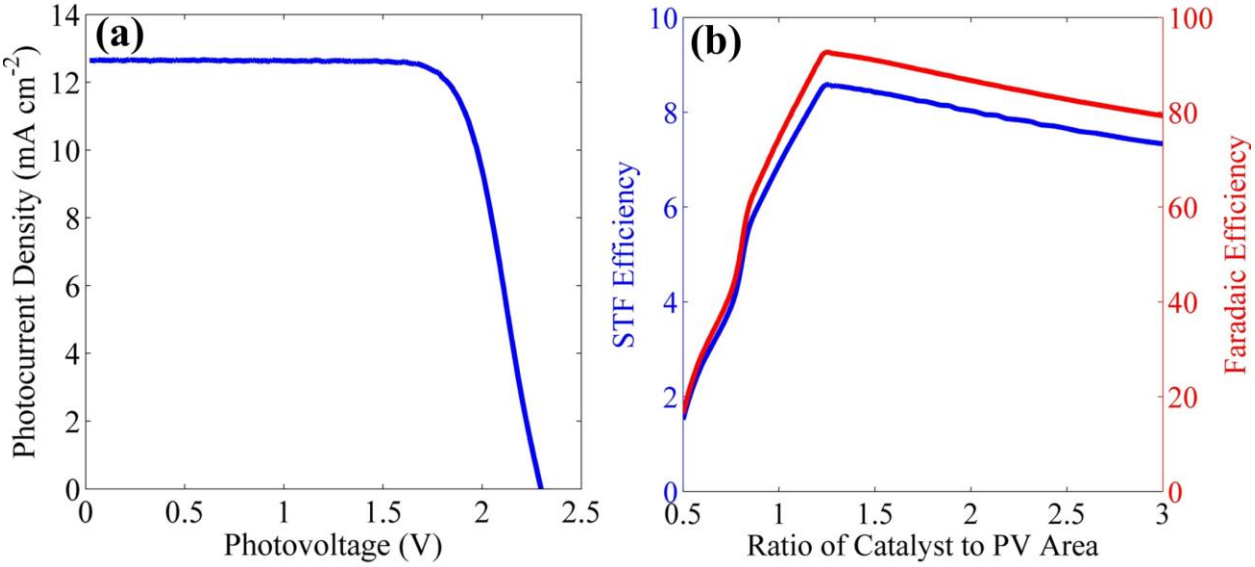

Figure S7: (a) Current density versus voltage (JV) characteristics of InGaP/GaAs/Ge triple-junction light absorber at AM 1.5, (b) variation in faradaic and STF efficiencies of CO formation on silver with the ratio of catalyst to PV area

S-11 Band-Gap Energies and Lattice Constants of Various Semiconductors and Alloys

Table S1 shows band-gap energies and lattice constants for commonly used group IV, II-V, and II-VI semiconductor materials.(7) The relevant semiconductor materials corresponding to the optimal band-gaps shown in Figures 3, 4, S3, S4, S5 and S6 can be found from Table S1, such that the selected semiconductor materials are lattice matched.

Table S1: Band-gaps and lattice constant of some commonly used group IV, III-V, and II-VI semiconductor materials

Material	Band-Gap (eV)	Lattice Constant (Å)
Sn	0.082	6.489
InSb	0.2	6.479
InAs	0.36	6.058
Ge	0.66	5.646
GaSb	0.72	6.096
$In_{0.53}Ga_{0.47}As$	0.74	5.869
Si	1.12	5.431
InP	1.35	5.869
GaAs	1.424	5.653
$Al_{0.48}In_{0.52}As$	1.46	5.869
CdTe	1.55	6.48
AlSb	1.58	6.135
CdSe	1.7	6.050
$In_{0.5}Ga_{0.5}P$	1.8	5.653
AlAs	2.17	5.66
GaP	2.26	5.451
$In_{0.5}Al_{0.5}P$	2.35	5.653
CdS	2.42	5.832
AlP	2.5	5.451
ZnSe	2.7	5.650
6H-SiC	2.996	3.086
GaN	3.36	3.189
ZnS	3.68	5.420
Diamond	5.47	3.567

S-12 Calculation of Electrolysis Efficiency and Profitability Index for Fuel Selection

The electrolysis efficiency is defined as the ratio of the thermoneutral potential to the applied potential. The reported values of electrolysis efficiency are derived for the applied potential of 2V, which corresponds to DOE target of 75% efficiency for hydrogen production.

The energy densities are calculated using the following formula.

$$\text{Energy Density}\left(\frac{\text{MJ}}{\text{L}}\right) = \frac{\text{LHV}\left(\frac{\text{kJ}}{\text{mol}}\right)\times\text{Density}\left(\frac{\text{g}}{\text{mL}}\right)}{\text{Molecular Weight}\left(\frac{\text{g}}{\text{mol}}\right)} \quad (8)$$

Table S2: Lower heating value (LHV), electrolysis efficiency, and density of various CO_2 reduction products

Product	**LHV (kJ/mol)**	**Electrolysis Efficiency @ 2 V**	**Density @ 1 atm (g/mL)**	**Density @ Elevated Pressure (g/mL)**	**Note**
Hydrogen	241.81	74.1	0.00008375	0.03122	50 MPa
Carbon Monoxide	282.98	73.3	0.001165	0.2667	25 MPa
Formic Acid	209.82	65.8	1.22	N/A	
Methanol	638.73	62.8	0.792	N/A	
Methane	802.23	57.7	0.0006682	0.1936	25 MPa
Ethanol	1322.94	59.1	0.789	N/A	
Ethene	1235.45	61.0	0.001173	0.4273	25 MPa
1-Propanol	1843.69	58.2	0.803	N/A	

The profitability index, defined as the ratio of economic value to the required electrical energy per mole of products, can be written as

$$\text{Profitability Index}\left(\frac{¢}{\text{kWh}}\right) = \frac{\text{Economic Value}\left(\frac{¢}{\text{mol product}}\right)}{\frac{\text{mol e}^-}{\text{mol product}} \times \text{Faraday Constant}\left(\frac{\text{C}}{\text{mol e}^-}\right) \times \text{Applied Potential}(\text{V})} \quad (9)$$

Table S3: Prices of various commercially available products

Product	**Source**	**Price per Container**	**Basis**	**¢ mol^{-1}**
Hydrogen	ICIS	$63.59	100 SCF	9.95
Carbon Monoxide	Alibaba	$1,215.65	100 45 L Cylinders @ 175 bar	1.91
Formic Acid	ICIS	$213.00	kg	31.56
Methanol	ICIS	$81.30	gal	3.77
Methane	US EIA	$1,283.19	1000 CF	0.004
Ethanol	ICIS	$216.50	gal	6.74
Ethene	ICIS	$1,204.35	lb	6.15
1-Propanol	Bloomberg	$168.50	lb	14.83

References

1. Henry CH (1980) Limiting efficiencies of ideal single and multiple energy gap terrestrial solar cells. *Journal of applied physics* 51(8):4494-4500.
2. Hu S, Xiang C, Haussener S, Berger AD, & Lewis NS (2013) An analysis of the optimal band gaps of light absorbers in integrated tandem photoelectrochemical water-splitting systems. *Energy & Environmental Science* 6(10):2984-2993.
3. Krebs K (1983) *Standard procedures for terrestrial photovoltaic performance measurements* (Springer).
4. Hatsukade T, Kuhl KP, Cave ER, Abram DN, & Jaramillo TF (2014) Insights into the electrocatalytic reduction of CO 2 on metallic silver surfaces. *Physical Chemistry Chemical Physics* 16(27):13814-13819.
5. Singh MR, Clark EL, & Bell AT (2015) Effects of electrolyte, catalyst, and membrane composition and operating conditions on the performance of solar-driven electrochemical reduction of carbon dioxide. *Physical Chemistry Chemical Physics* 17(29):18924-18936.
6. Karam NH, *et al.* (1999) Development and characterization of high-efficiency Ga 0.5 In 0.5 P/GaAs/Ge dual-and triple-junction solar cells. *Electron Devices, IEEE Transactions on* 46(10):2116-2125.
7. Kiyoshi T, Akihiko Y, & Adarsh S (2007) Wide Bandgap Semiconductors: Fundamental Properties and Modern Photonic and Electronic Devices. (Springer, Heidelberg).